RSC Advances

PAPER

View Article Online
View Journal | View Issue

Cite this: *RSC Adv.*, 2023, **13**, 31667

Electrospun VO_2/carbon fibers for aqueous zinc-ion batteries

Liying Yin,[a] Zenglong Xu,[b] Guangxu Yang,[b] Fuhai Guo,[a] Wenhui Guo,[a] Songfang Zhao*[b] and Shuhua Yang *[b]

Received 20th September 2023
Accepted 24th October 2023

DOI: 10.1039/d3ra06395j

rsc.li/rsc-advances

Aqueous zinc-ion batteries (AZIBs) have become one of the most potential energy storage devices due to their high safety and low cost. Vanadium oxide is an ideal cathode material for AZIBs because of its unique tunnel structure and multivalent nature. In this work, electrospun VO_2/carbon fibers (VO_2@CPAN) with a three-dimensional (3D) network are obtained by an electrospinning strategy combining with a controlled heat treatment. As cathode for AZIBs, the 3D network of the carbon fiber significantly improves the conductivity of VO_2, avoids the agglomeration of VO_2, and increases the stability of VO_2. Therefore, VO_2@CPAN delivers a specific capacity of 323.2 mA h g^{-1} at 0.2 A g^{-1}, which is higher than pure VO_2. At the same time, excellent capacity retention of 76.6% is obtained at high current density of 10 A g^{-1} after 3000 cycles.

1. Introduction

Aqueous zinc-ion batteries (AZIBs) have gradually attracted worldwide attention due to their advantages of simple processing, high safety, and environmental friendliness.[1–4] At present, a variety of AZIBs cathode materials have been developed, including manganese-based compounds, vanadium-based compounds, Prussian blue analogues, *etc.*[5–9] Among the various cathode materials, vanadium-based materials have great potential for developing high-performance AZIBs due to their multivalence nature and versatile vanadium oxide frameworks.[10–13] However, the relatively poor conductivity of VO_2 hinders the electron transport, thus limiting its electrochemical performance.[14–17] Some strategies have been proposed to improve the conductivity of VO_2, among which combining conductive materials, such as polyaniline (PANI), polypyrrole (PPy), and poly(3,4-ethylenedioxythiophene) (PEDOT), is an effective method.[18–21] These materials show improved conductivity and stabilized structure by wrapping or embedding VO_2. Recently, the oxygen-deficient hydrate vanadium dioxide with polypyrrole coating (O_d-HVO@PPy) is developed, in which the conductive polymer coating enhances the electronic transfer and suppresses the cathode dissolution.[22] Gu *et al.* reported nitrogen-doped VO_2(B) nanobelts (VO_2-N) and carbon-coated VO_2 nanobelts (VO_2@C), presenting superior electrochemical performances to those of pure VO_2(B) in AZIBs.[23,24] Liu *et al.* developed K^+ pre-intercalated V_2O_5, carbon-coated V_2O_5 microspheres, and V_6O_{13}/VO_2 electrode materials, which also exhibit improved electrochemical performance for AZIBs.[25–27] Although some achievements have been made, improving the ions diffusion and architecture stability of VO_2 to achieve high-performance AZIBs is still a much-needed study. For improving the electronic conductivity and structural durability of VO_2, carbon fiber is particularly promising due to large specific surface area, great conductivity, and superior stability.

Herein, VO_2 was first prepared by hydrothermal method, and then VO_2 was embedded in carbon fiber by an electrospinning strategy combining with a controlled heat treatment. The obtained electrospun VO_2/carbon fibers (VO_2@CPAN) consists of carbon fibers with three-dimensional (3D) network structure and flake-like VO_2. The 3D network carbon fibers significantly improve the conductivity of the electrode and the flake-like VO_2 provides more active sites for electrochemical reactions. The VO_2@CPAN cathode achieves a high specific capacity of 323.2 mA h g^{-1} at a current density of 0.2 A g^{-1}, which is much higher than the pure VO_2 cathode. In addition, an impressive capacity retention rate of 76.6% is obtained after 3000 cycles at a high current density of 10 A g^{-1}.

2. Experimental

2.1. Synthesis of VO_2 and VO_2@CPAN

For VO_2, 2.2 g of Na_3VO_4 was added to 60 mL of deionized water, accompanied by stirring for 15 min at room temperature, and then 10 mL of ethylene glycol was added and stirred for another 30 min. The pH of the above solution was adjusted to 2 with 2 M HCl. The mixed solution was stirred for 45 minutes at 75 °C, then moved into a 100 mL Teflon-lined stainless steel autoclave and heated to 180 °C for 7 h. VO_2 was obtained after washing with deionized water and ethanol, followed by vacuum drying at 60 °C.

[a]*School of Food Science and Engineering, Changchun University, Changchun 130022, China*

[b]*Materials Center for Energy and Photoelectrochemical Conversion, School of Material Science and Engineering, University of Jinan, Jinan 250022, China. E-mail: yangshuhua78@163.com; mse_zhaosf@ujn.edu.cn*

For electrospun VO_2/carbon fibers (VO_2@CPAN), 0.3 g of the obtained VO_2 powder was dissolved in to 10 mL of *N*,*N*-dimethylformamide (DMF) solution with 10% polyacrylonitrile (PAN), then was stirred at 45 °C for 12 h. The above solution was transferred to a 10 mL of plastic syringe with a 19-gauge blunt tip needle. Electrospinning was carried out in an electrospinning equipment (SS-2535H, Ucalery). The applied voltage is 20 kV, the distance from needle to collector is 15 cm, and the flow rate is 0.05 mm min^{-1}. The as-collected electrospun fibers was first heated to 280 °C in air at a heating rate of 1 °C min^{-1} and kept for 2 h. After that, it was heated to 500 °C at a heating rate of 5 °C min^{-1} in a nitrogen atmosphere and kept for 1 h. Finally, it was heated to 700 °C at a heating rate of 5 °C min^{-1} and kept for 2 h. After natural cooling, electrospun VO_2/carbon fibers (VO_2@CPAN) are obtained. The pure carbon fibers (CPAN) are prepared by the similar process to VO_2@CPAN except no adding VO_2 in electrospinning solution.

2.2. Material characterizations

The crystal structures of VO_2@CPAN were characterized by an X-ray diffractometer (D8 FOCUS) with a Cu target. The morphology and microstructure of the samples were observed by a field-emission scanning electron microscope (SEM, Quanta 250 FEG, FEI).

2.3. Electrochemical measurements

The electrochemical performance of Zn//VO_2@CPAN AZIBs was studied in a CR2032-type coin cells assembled in air. The VO_2@CPAN cathode was prepared by mixing VO_2@CPAN powder, conductive carbon, and polyvinylidene fluoride (PVDF) with a mass ratio of 7 : 2 : 1 in *N*-methyl-2-pyrrolidone (NMP), fully grinding in the bowl, coating on the graphite paper and drying at 60 °C for 12 h. The mass of active materials of on current collector was about 2 mg cm^{-2}. The glass fiber membrane was used as the separator, a zinc foil was used as the anode, and 2 M $ZnSO_4$ solution was used as the electrolyte.

Cyclic voltammetry (CV) and electrochemical impedance spectroscopy (EIS) were carried out using a Zahner/Zennium electrochemical workstation. The galvanostatic charge–discharge (GCD) curves and the specific capacity were obtained with a NEWARE battery testing system (CT-4008Tn-5V10mA). CV and GCD were conducted from 0.20 to 1.35 V (*vs.* Zn^{2+}/Zn).

3. Results and discussion

The preparation process of electrospun VO_2/carbon fibers (VO_2@CPAN) is shown in Fig. 1. Firstly, the pure VO_2 powder was synthesized by simple hydrothermal method. Then, the obtained VO_2 powder was dissolved in the solution of *N*,*N*-dimethylformamide (DMF) and polyacrylonitrile (PAN) to be electrospun into VO_2/PAN fibers, which was converted into VO_2/carbon fibers (VO_2@CPAN) *via* a controlled heat treatment.

Fig. 2 shows the PAN fibers obtained by electrospinning and the CPAN after a controlled heat treatment. It can be seen that both fibers have a uniform diameter of about 200 nm. The VO_2 synthesized by simple hydrothermal method presents a disordered flake structure with a width of more than 200 nm, accompanied by severe agglomeration (Fig. 3a and b). The

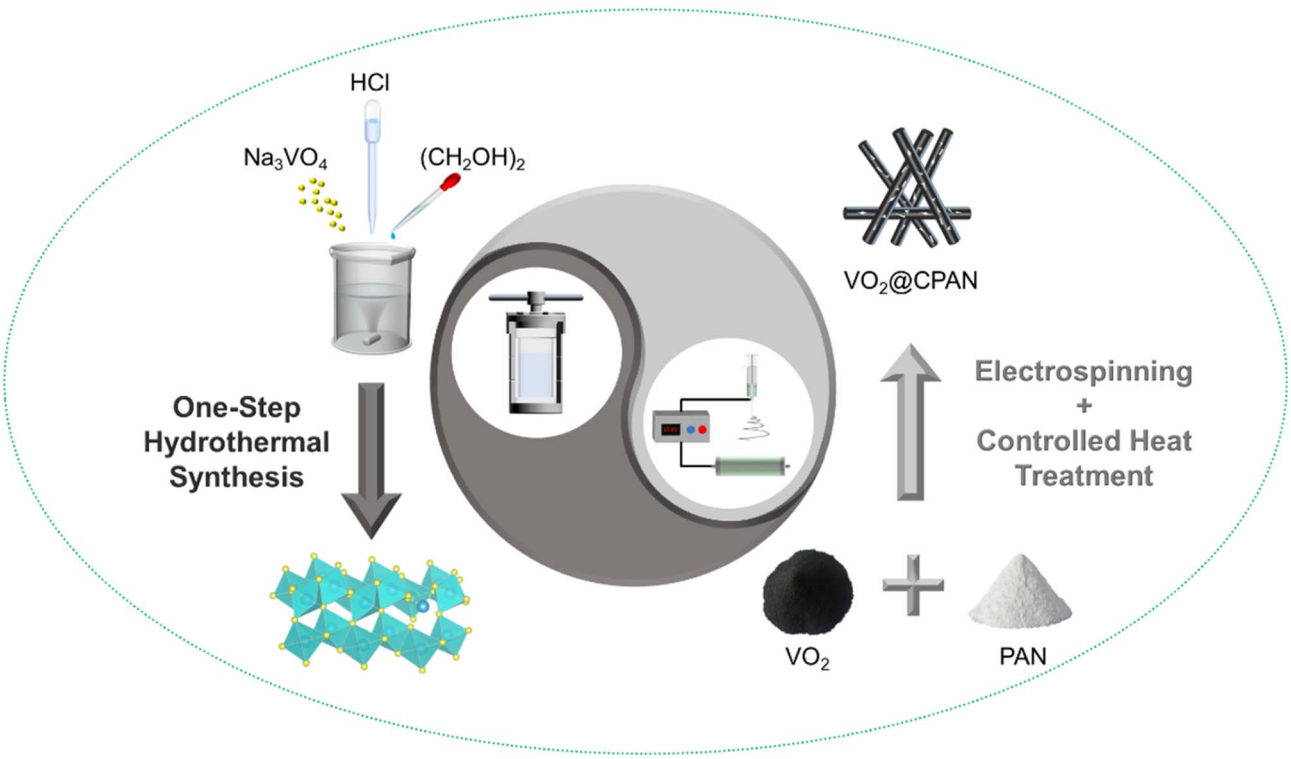

Fig. 1 Schematic illustration of preparation process for VO_2@CPAN.

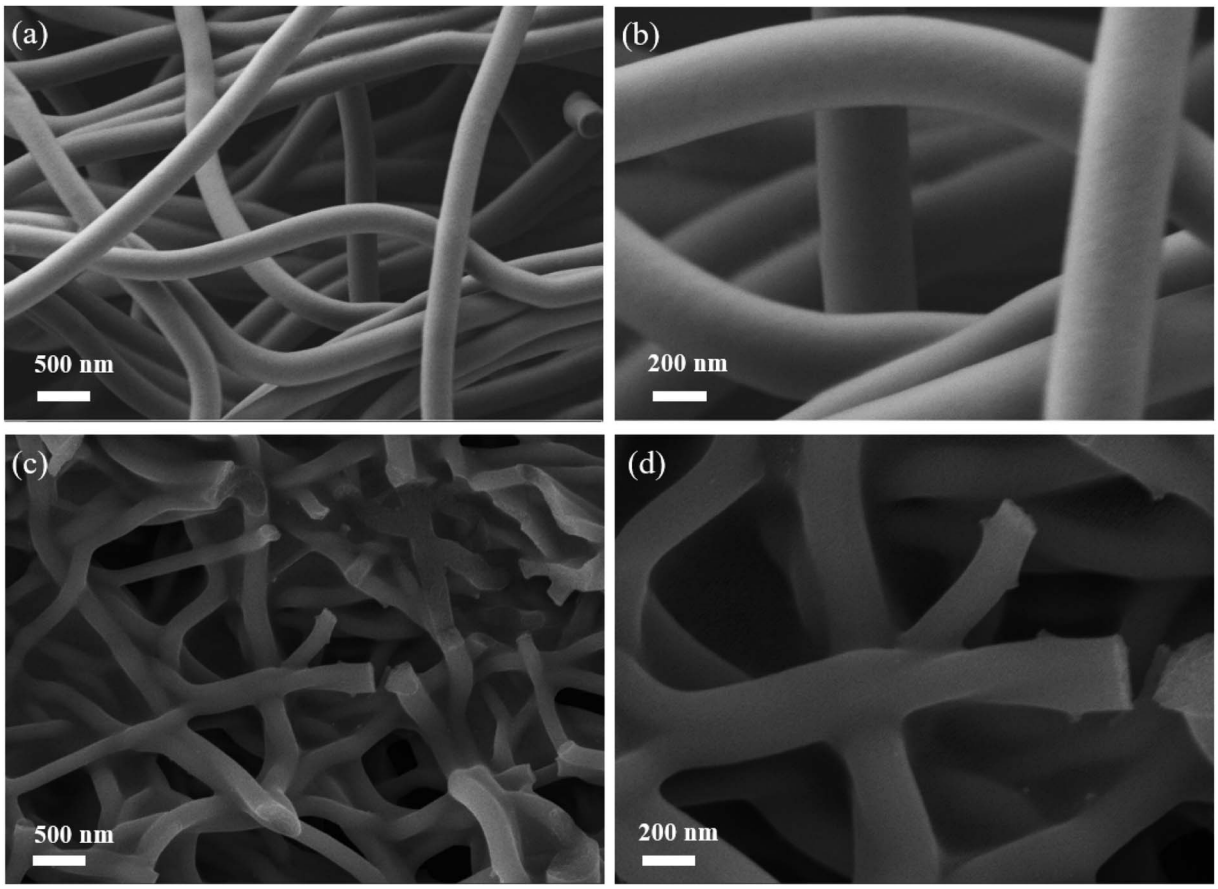

Fig. 2 SEM images of (a and b) PAN fibers and (c and d) CPAN.

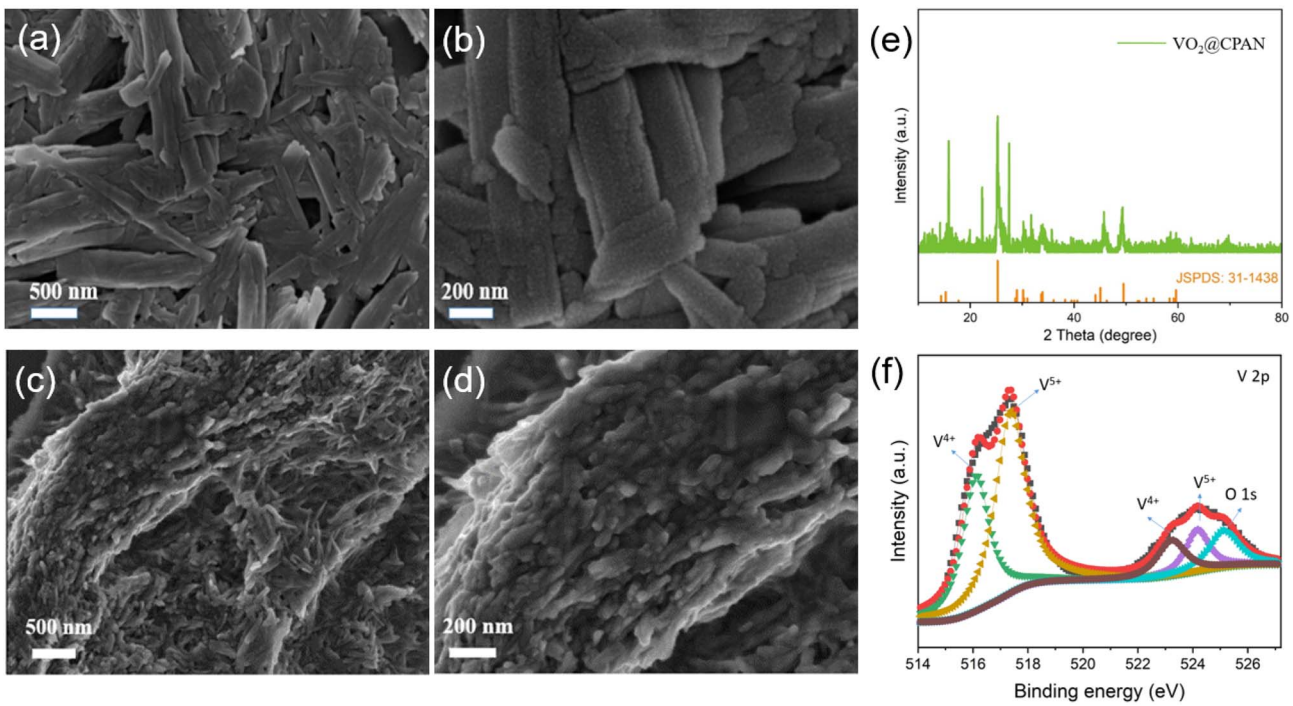

Fig. 3 SEM images of (a and b) VO_2 and (c and d) VO_2@CPAN; (e) XRD of VO_2@CPAN; (f) high-resolution XPS V 2p spectra for VO_2@CPAN.

presence of agglomeration could lead to a lack of full contact between the active material and the electrolyte, limiting the complete utilization of the active material. When the VO_2 nanosheets were combined with the carbon fibers *via* an electrospinning strategy combining with a controlled heat treatment, it can be clearly seen that the VO_2 nanosheets are uniformly embedded in the carbon fibers and the diameter of the VO_2@CPAN composite fibers increase to 1.1 μm (Fig. 3c and d). The 3D network carbon fibers significantly improve the conductivity of the electrode and effectively reduce the agglomeration phenomenon of VO_2 nanosheets. Also, this 3D network with abundant porosity can greatly improve ion transfer kinetics during the charge–discharge process.[28] The flake-like VO_2 provides more active sites for electrochemical reactions, making AZIBs obtain high energy storage.[29] The close contact between carbon fibers and VO_2 nanosheets establishes an interconnection network with high stability for electrochemical reactions, which effectively improves the cycling life of AZIBs. In order to investigate whether VO_2 changes before and after recombination with carbon fiber, the crystal structure of VO_2@CPAN was analyzed by X-ray diffraction (XRD). As shown in Fig. 3e, one main peak at 23° in the XRD pattern of VO_2@CPAN can be attributed to the carbon fibers, and other peaks are consistent with the monoclinic phase VO_2(B) (JSPDS No. 31-1438). For the V 2p XPS spectrum of VO_2@CPAN (Fig. 3f), the characteristic peaks at 516.1 (523.3) eV and 517.5 (524.2) eV attributed to V^{4+}/V^{5+}, respectively. The presence of V^{5+} is due to surface oxidation caused by air atmosphere,[30] which is in accord with the less impure peaks appeared in the XRD pattern. This shows that the crystal structure of VO_2 after combing with carbon fibers has no obvious change.

In order to evaluate the electrochemical performance of the VO_2@CPAN, Zn//VO_2@CPAN AZIBs were assembled with VO_2@CPAN as cathode, Zn foil as anode, and 2 M $ZnSO_4$ solution as electrolyte. The cyclic voltammetry (CV) curves of Zn//VO_2@CPAN and Zn//VO_2 AZIBs are shown in Fig. 4a. They have similar redox peaks and Zn//VO_2@CPAN batteries exhibit a larger current response, indicating that the 3D network

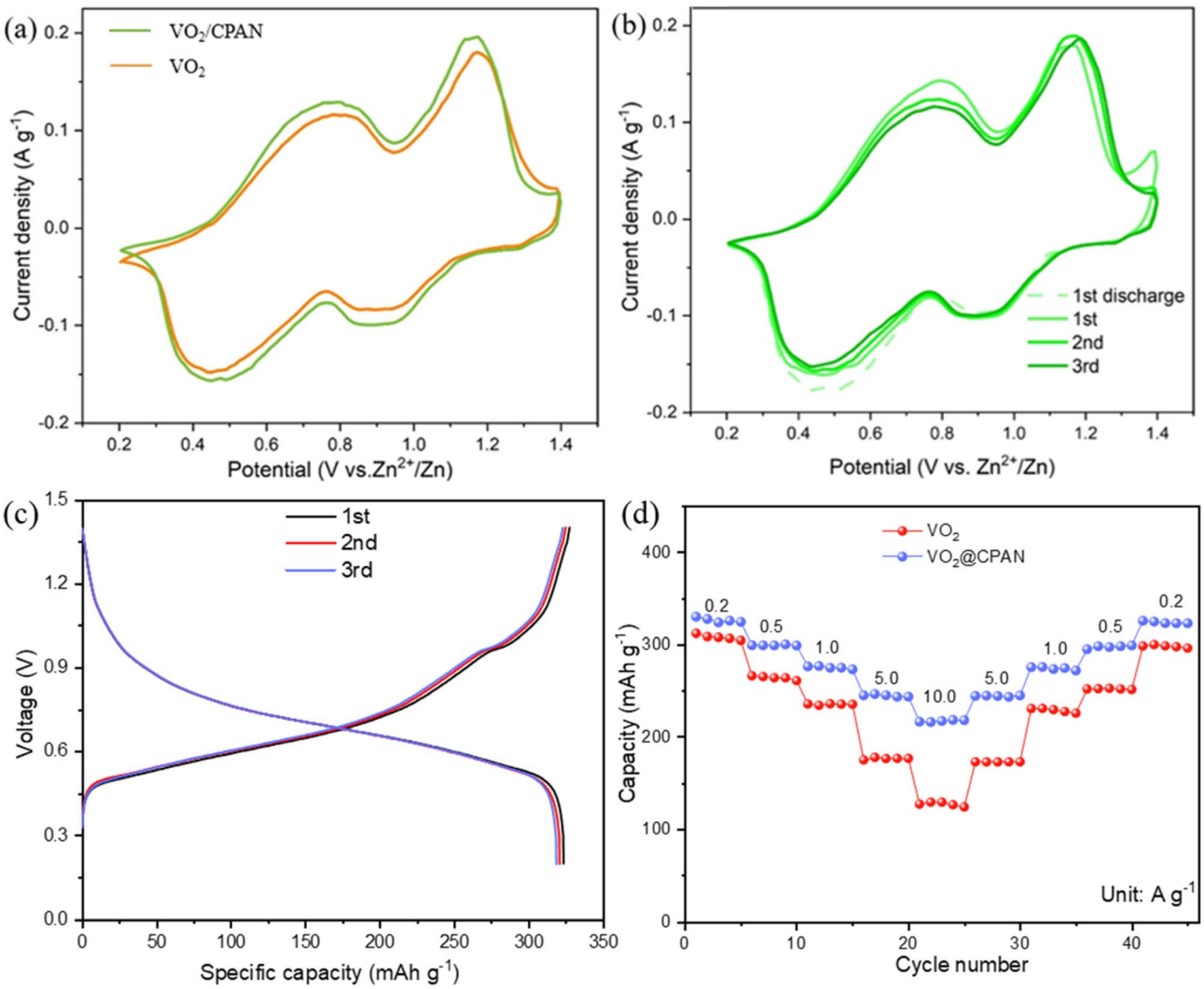

Fig. 4 (a) CV curves of Zn//VO_2@CPAN and Zn//VO_2 AZIBs at 0.2 mV s^{-1}; (b) CV curves of Zn//VO_2@CPAN AZIBs at 0.2 mV s^{-1}; (c) GCD curves of Zn//VO_2@CPAN AZIBs at 0.2 A g^{-1}; (d) rate performances of Zn//VO_2@CPAN and Zn//VO_2 AZIBs.

carbon fibers can effectively enhance the electrochemical activity of VO_2 nanosheets. Two pairs of redox peaks at around 0.75/0.47 V and 1.15/0.9 V correspond to zinc ion extraction/insertion and V^{3+}/V^{4+} redox processes, respectively.[31] As shown in Fig. 4b, the CV curves of the second and third cycles are basically consistent with the first curve, indicating that the VO_2@CPAN electrode has excellent reversibility. In addition, the galvanostatic charge–discharge (GCD) curves (Fig. 4c) of the Zn//VO_2@CPAN AZIBs at 0.2 A g^{-1} show that the second and third discharge/charging curves are highly consistent with the first cycle, which also indicates that VO_2@CPAN has superior reversibility and stability as a cathode material. Fig. 4d shows the rate capability of the Zn//VO_2@CPAN AZIBs. The specific capacities of Zn//VO_2@CPAN AZIBs at 0.2, 0.5, 1.0, 5.0 and 10.0 A g^{-1} are 326.5, 299.6, 275.4, 244.8 and 217.3 mA h g^{-1}, respectively. When the current density returns to 0.2 A g^{-1}, the capacity can reach 324.1 mA h g^{-1}, which is equivalent to 99.2% of the initial capacity and higher than the Zn//VO_2 AZIBs (96.6%). The improvement of rate performance is attributed to 3D network of VO_2@CPAN, which provides ample channel for the rapid ion transport.

As shown in Fig. 5a, electrochemical impedance spectroscopy (EIS) shows that Zn//VO_2@CPAN has a smaller semicircular arc in the high-frequency region, indicating the smaller charge transfer resistance between the VO_2@CPAN electrode and the electrolyte.[32] This proves that the 3D network carbon fibers provide a direct electron/ion transport pathway, guaranteeing the fast charge transfer and ion exchange in VO_2@CPAN. As shown in Fig. 5b, the long-term cycling performance of Zn//VO_2@CPAN AZIBs at 0.2 A g^{-1} was tested. Zn//VO_2@CPAN AZIBs exhibited 92.2% capacity retention, whereas Zn//VO_2 AZIBs presented a capacity retention rate of only 80.1% after 100 cycles. This shows that the performance of Zn//VO_2@CPAN AZIBs has been comprehensively improved. Even at a high current density of 10 A g^{-1}, Zn//VO_2@CPAN batteries still achieve a high initial capacity of 217.3 mA h g^{-1} with a capacity retention of 76.6% after 3000 cycles, much better than Zn//VO_2 batteries (Fig. 5c). The 3D network in the VO_2@CPAN increases the specific surface area of the active material for the electrolyte access and avoids the agglomeration phenomenon of VO_2, which can bring more reaction sites for the electrochemical reaction. Therefore, the electrochemical performance of Zn//VO_2@CPAN battery is improved. In addition, at a power density of 375 W kg^{-1}, Zn//VO_2@CPAN AZIBs delivered an energy density of 225 W h kg^{-1}. As shown in Ragone plot (Fig. 5d), VO_2@CPAN reveals a competitive performance in comparison with other previously reported materials, such as $V_2O_5 \cdot 4VO_2 \cdot 2.72H_2O$,[33] Nsutite-type VO_2 microcrystals,[34] HVO,[35] Ancient Chinese Coin-shaped VO_2,[36] $Li_xV_2O_5 \cdot nH_2O$,[37] $Na_3V_2(PO_4)_2$,[38] V_2O_5,[39] VS_2,[40] $H_2V_3O_8$,[41] $Zn_{0.25}V_2O_5 \cdot nH_2O$.[42]

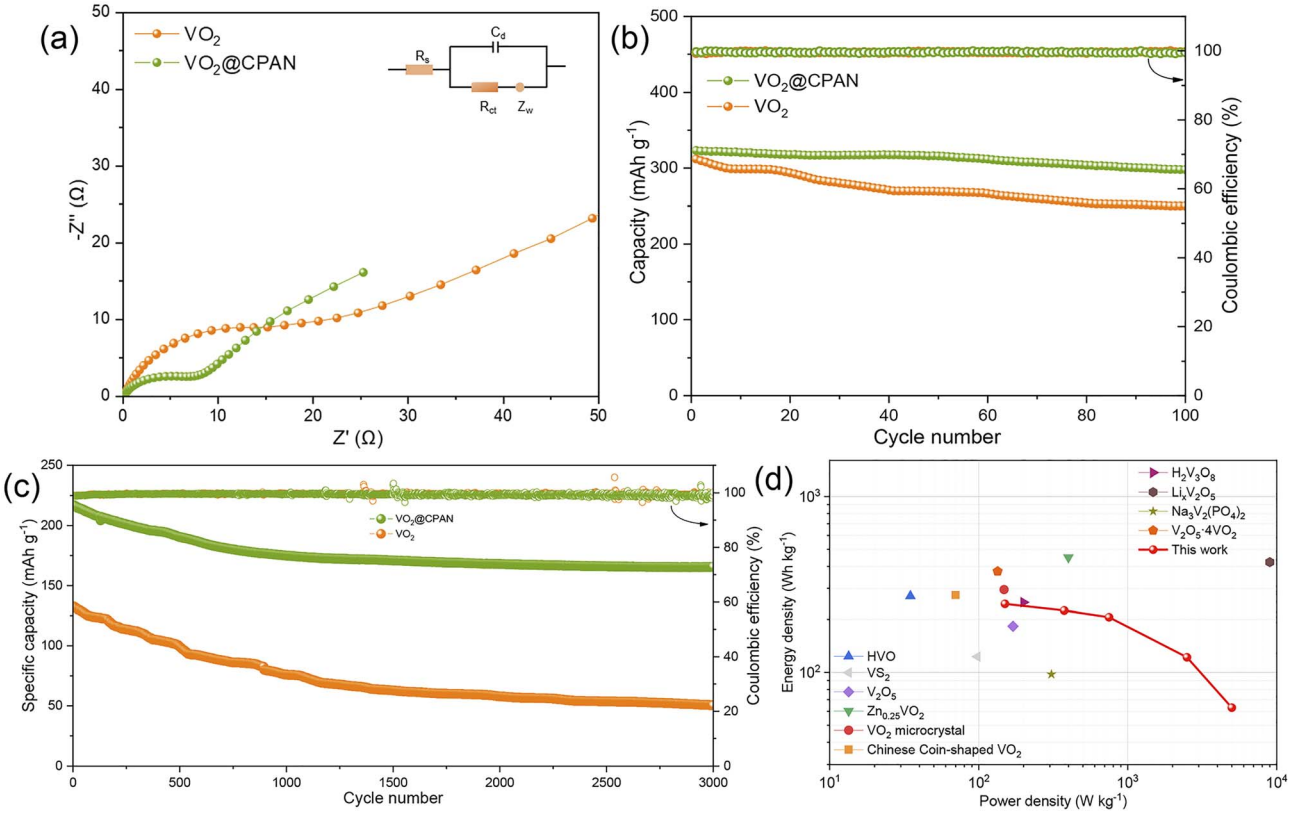

Fig. 5 (a) EIS, cyclic performance and coulombic efficiency at (b) 0.2 A g^{-1} and (c) 10 A g^{-1} for Zn//VO_2@CPAN and Zn//VO_2 AZIBs; (d) Ragone plot of the Zn//VO_2 AZIBs and other vanadium-based AZIBs.

4. Conclusions

In summary, electrospun VO_2/carbon fibers (VO_2@CPAN) with a three-dimensional (3D) network were successfully prepared by an electrospinning strategy combining with a controlled heat treatment. The 3D network not only improved the conductivity of VO_2, but also avoided the agglomeration of VO_2 and provided ample channel for the rapid ion transport. In addition, the flake-like VO_2 provides more active sites for electrochemical reactions. Therefore, the VO_2@CPAN cathode achieves a high specific capacity of 323.2 mA h g^{-1} at a current density of 0.2 A g^{-1}, which is much higher than the pure VO_2 cathode. At a high current density of 10 A g^{-1}, the Zn//VO_2@CPAN battery delivered a high specific capacity of 217.3 mA h g^{-1} and still maintained 76.6% capacity retention after 3000 cycles. The strategy of designing 3D electrospun VO_2/carbon fibers by electrospinning provides a new method for constructing advanced cathode for AZIBs.

Conflicts of interest

There are no conflicts to declare.

Acknowledgements

This work is supported by Shandong Provincial Natural Science Foundation (ZR2022ME181), NSFC (51702123), University of Jinan Science and Technology Planning Project (XKY2034). S. Y. thanks the start-up research funding from University of Jinan.

Notes and references

1 M. Liu, D. Zhang, B. Liu, C. Tian, B. Zhao, Y. Wang, Y. Wang, Y. Hu, L. Kong, D. Luo and Z. Chen, *Nano Energy*, 2022, **103**, 107795.
2 Y. Zhang, A. Chen and J. Sun, *J. Energy Chem.*, 2021, **54**, 655–667.
3 S. Yang, Y. Cui, G. Yang, S. Zhao, J. Wang, D. Zhao, C. Yang, X. Wang and B. Cao, *J. Power Sources*, 2023, **554**, 232347.
4 J. Zhang, J. Zhao, H. Du, Z. Zhang, S. Wang and G. Cui, *Electrochim. Acta*, 2018, **280**, 108–113.
5 H. Wang, W. Yang, H. Xu, M. Li, H. Liu, S. Gong, F. Zhao, C. Li, J. Qi, W. Peng and J. Liu, *Small*, 2023, 2304504.
6 J. Liu, P. Xu, J. Liang, H. Liu, W. Peng, Y. Li, F. Zhang and X. Fan, *Chem. Eng. J.*, 2020, **389**, 124405.
7 S. Zuo, J. Liu, W. He, S. Osman, Z. Liu, X. Xu, J. Shen, W. Jiang, J. Liu, Z. Zeng and M. Zhu, *J. Phys. Chem. Lett.*, 2021, **12**, 7076–7084.
8 Y. Du, X. Wang and J. Sun, *Nano Res.*, 2020, **14**, 754–761.
9 Z. Luo, J. Zeng, Z. Liu and H. He, *J. Alloys Compd.*, 2022, **906**, 164388.
10 Z. Zhang, S. Li, X. Zhang, Y. Du, Z. Wen, S. Ji and J. Sun, *Mater. Lett.*, 2021, **301**, 130259.
11 Y. Wang, L. Zhou, X. Cao, X. Gao and X. Lu, *J. Mater. Chem. A*, 2021, **9**, 26698–26703.
12 P. Oberholzer, E. Tervoort, A. Bouzid, A. Pasquarello and D. Kundu, *ACS Appl. Mater. Interfaces*, 2018, **11**, 674–682.
13 Z. Chen, J. Hu, T. He, C. Feng, Y. Luo, H. Hou, G. Zou and X. Ji, *Energy Storage Mater.*, 2022, **50**, 1–11.
14 F. Wu, Y. Jiang, Z. Ye, Y. Huang, Z. Wang, S. Li, Y. Mei, M. Xie, L. Li and R. Chen, *J. Mater. Chem. A*, 2019, **7**, 1315–1322.
15 Z. Wang, K. Yu, Y. Feng, R. Qi, J. Ren and Z. Zhu, *ACS Appl. Mater. Interfaces*, 2019, **11**, 44282–44292.
16 K. Zhu, T. Wu and K. Huang, *ACS Nano*, 2019, **13**, 14447–14458.
17 X. Li, L. Yang, H. Mi, H. Li, M. Zhang, A. Abliz, F. Zhao, S. Wang and H. Li, *CrystEngComm*, 2021, **23**, 8650–8659.
18 J. Wu, W. Xu, Y. Lin, X. Shi, F. Yang and X. Lu, *J. Power Sources*, 2021, **483**, 229114.
19 R. Venkatkarthick, N. Rodthongkum, X. Zhang, S. Wang, P. Pattananuwat, Y. Zhao, R. Liu and J. Qin, *ACS Appl. Energy Mater.*, 2020, **3**, 4677–4689.
20 Y. Liu, Y. Jiang, Z. Hu, J. Peng, W. Lai, D. Wu, S. Zuo, J. Zhang, B. Chen, Z. Dai, Y. Yang, Y. Huang, W. Zhang, W. Zhao, W. Zhang, L. Wang and S. Chou, *Adv. Funct. Mater.*, 2020, **31**, 2008033.
21 X. Liu, G. Xu, Q. Zhang, S. Huang, L. Li, X. Wei, J. Cao, L. Yang and P. K. Chu, *J. Power Sources*, 2020, **463**, 228223.
22 Z. Zhang, B. Xi, X. Wang, X. Ma, W. Chen, J. Feng and S. Xiong, *Adv. Funct. Mater.*, 2021, **31**, 2103070.
23 X. Gu, J. Wang, X. Zhao, X. Jin, Y. Jiang, P. Dai, N. Wang, Z. Bai, M. Zhang and M. Wu, *J. Energy Chem.*, 2023, **85**, 30–38.
24 X. Gu, J. Wang, S. Wu, S. Dong, F. Li, A. Cui, M. Zhang, P. Dai and M. Wu, *Mater. Adv.*, 2023, DOI: **10.1039/D3MA00622K**.
25 Y. Liu, Y. Liu, X. Wu and Y.-R. Cho, *ACS Sustainable Chem. Eng.*, 2023, **11**, 13298–13305.
26 Y. Liu, Y. Liu, X. Wu and Y.-R. Cho, *J. Colloid Interface Sci.*, 2022, **628**, 33–40.
27 Y. Liu and X. Wu, *J. Energy Chem.*, 2023, **87**, 334–341.
28 Z.-T. Wang, R.-C. Wang, L.-B. Tang, Y.-J. Li, J. Mao, K.-H. Dai, Z.-J. He and J.-C. Zheng, *Solid State Ionics*, 2021, **369**, 115714.
29 S. J. Kim, C. R. Tang, G. Singh, L. M. Housel, S. Yang, K. J. Takeuchi, A. C. Marschilok, E. S. Takeuchi and Y. Zhu, *Chem. Mater.*, 2020, **32**, 2053–2060.
30 T. Wei, Q. Li, G. Yang and C. Wang, *J. Mater. Chem. A*, 2018, **6**, 8006–8012.
31 X. Dai, F. Wan, L. Zhang, H. Cao and Z. Niu, *Energy Storage Mater.*, 2019, **17**, 143–150.
32 G. Yang, S. Yang, J. Shen, Y. Cui, J. Sun, G. Duan, B. Cao and Z. Liu, *ACS Appl. Energy Mater.*, 2023, **6**, 1871–1876.
33 T.-T. Lv, Y.-Y. Liu, H. Wang, S.-Y. Yang, C.-S. Liu and H. Pang, *Chem. Eng. J.*, 2021, **411**, 128533.
34 Y.-Y. Liu, T.-T. Lv, H. Wang, X.-T. Guo, C.-S. Liu and H. Pang, *Chem. Eng. J.*, 2021, **417**, 128408.
35 N. Liu, X. Wu, L. Fan, S. Gong, Z. Guo, A. Chen, C. Zhao, Y. Mao, N. Zhang and K. Sun, *Adv. Mater.*, 2020, **32**, 1908420.
36 Z. Cao, L. Wang, H. Zhang, X. Zhang, J. Liao, J. Dong, J. Shi, P. Zhuang, Y. Cao, M. Ye, J. Shen and P. M. Ajayan, *Adv. Funct. Mater.*, 2020, **30**, 2000472.
37 Y. Yang, Y. Tang, G. Fang, L. Shan, J. Guo, W. Zhang, C. Wang, L. Wang, J. Zhou and S. Liang, *Energy Environ. Sci.*, 2018, **11**, 3157–3162.

38 G. Lin, R. Ma, Y. Zhou, Q. Liu, X. Dong and J. Wang, *Electrochim. Acta*, 2018, **261**, 49–57.
39 P. Hu, M. Yan, T. Zhu, X. Wang, X. Wei, J. Li, L. Zhou, Z. Li, L. Chen and L. Mai, *ACS Appl. Mater. Interfaces*, 2017, **9**, 42717–42722.
40 P. He, M. Yan, G. Zhang, R. Sun, L. Chen, Q. An and L. Mai, *Adv. Energy Mater.*, 2017, **7**, 1601920.
41 P. He, Y. Quan, X. Xu, M. Yan, W. Yang, Q. An, L. He and L. Mai, *Small*, 2017, **13**, 1702551.
42 D. Kundu, B. D. Adams, V. Duffort, S. H. Vajargah and L. F. Nazar, *Nat. Energy*, 2016, **1**, 16119.